

Mapping Return Levels of Absolute NDVI Variations for the Assessment of Drought Risk in Ethiopia

Francesco Tonini^{a, *}, Giovanna Jona Lasinio^b, Hartwig H. Hochmair^a

^a *University of Florida, Fort Lauderdale Research and Education Center, 3205 College Avenue, Davie, Florida, 33314, U.S.A.*

^b *DSS, University of Rome "La Sapienza". P.le Aldo Moro 5, 00185 Rome, Italy.*

**Corresponding author. Tel.: +1 954 577 6392; fax: +1 954 424 6851.*

E-mail addresses: ftonini@ufl.edu (Francesco Tonini), giovanna.jonalasinio@uniroma1.it (Giovanna Jona Lasinio), hhhochmair@ufl.edu (Hartwig H. Hochmair).

Abstract

The analysis and forecasting of extreme climatic events has become increasingly relevant to planning effective financial and food-related interventions in third-world countries. Natural disasters and climate change, both large and small scale, have a great impact on non-industrialized populations who rely exclusively on activities such as crop production, fishing, and similar livelihood activities. It is important to identify the extent of the areas prone to severe drought conditions in order to study the possible consequences of the drought on annual crop production. In this paper, we aim to identify such areas within the South Tigray zone, Ethiopia, using a transformation of the Normalized Difference Vegetation Index (NDVI) called Absolute Difference NDVI (ADVI). Negative NDVI shifts from the historical average can generally be linked to a reduction in the vigor of local vegetation. Drought is more likely to increase in areas where negative shifts occur more frequently and with high magnitude, making it possible to spot critical situations. We propose a new methodology for the assessment of drought risk in areas where crop production represents a primary source of livelihood for its inhabitants. We estimate ADVI return levels pixel

per pixel by fitting extreme value models to independent monthly minima. The study is conducted using SPOT-Vegetation (VGT) ten-day composite (S10) images from April 1998 to March 2009. In all short-term and long-term predictions, we found that central and southern areas of the South Tigray zone are prone to a higher drought risk compared to other areas.

Keywords: drought risk, SPOT-Vegetation, NDVI, autocorrelation, return levels, extreme value distributions

1. Introduction

This study was conducted in collaboration with the United Nations World Food Programme (WFP). Before making any decisions and intervening in a country, the WFP needs to differentiate between emergency and non-emergency situations. Vulnerability Analysis and Mapping (VAM) is the common name given to the WFP's food security analysis work, which aims to identify and locate vulnerable people who may starve as a consequence of a crisis or natural disaster (United Nations World Food Programme, 2011).

Extreme natural and climatic events such as floods, hurricanes, and severe drought can put at high risk a large number of people who rely mainly on their own yield production to survive. The problems caused by such events and the need for quick intervention plans are an important push for improving early warning systems with new methodologies and appropriate statistical tools.

In contrast to other natural hazards, drought has a gradual onset and may last for several years, severely affecting agriculture and water supplies. Several definitions of drought can be found depending on the specific way it is measured. The National Aeronautics and Space Administration's Earth Observatory (NASA Earth Observatory, 2011) defines drought according to agricultural, meteorological, and hydrological criteria. *Agricultural drought* takes place when soil lacks moisture that a specific crop would need at a specific time. *Meteorological drought* is caused by negative deviations of long-term precipitation from the norm. *Hydrological drought* is caused by lack of sufficient surface and subsurface water supplies. Agricultural drought typically manifests after a

meteorological drought and before a hydrological drought. Persendt (2009) defines the concept of *socioeconomic* drought, which becomes evident when physical water scarcity starts affecting people's lives.

In African countries drought tends to encompass large areas and, at the same time, ground-based meteorological stations are sparse or non-existent. Satellite data provide a powerful alternative to ground-based weather measurements because they are able to cover an entire region (Wardlow, 2009). In this study, we model drought risk within the South Tigray zone, Ethiopia, using SPOT-Vegetation (VGT) ten-day composite (S10) images from April 1998 to March 2009. We use a satellite-based indicator called Absolute Difference NDVI (ADVI), a simple transformation of the Normalized Difference Vegetation Index (NDVI) measuring shifts of actual values from their historical average. The main scope of the study is to assess which areas are more prone to drought events considering their recent histories.

The remainder of this paper provides a brief overview of existing drought risk assessment methods and proposes a new approach based on the Extreme Value Theory (EVT). A detailed case study is then presented where different EVT models are tested and compared.

2 Methodologies

The assessment of drought conditions is more accurate when the variable of interest is measured *in situ*, i.e., recorded directly at a series of ground stations where the event under study is happening. Ideally, ground stations would be uniformly located and closely spaced in order to get the best information. However, in most cases the costs associated with a dense spatial coverage are high and third-world countries rarely have the economic and human resources necessary to realize this ideal situation. Most modern satellites are able to provide continuous, consistent, and accurate measurements at a high spatial coverage which can be integrated with *in situ* observations or replace them entirely (NOAA National Climatic Data Center, 2011). Accuracy of measurements

depends on several factors such as atmospheric interferences, sensor calibration, and both spatial and spectral resolutions (Jensen, 2005).

Existing literature suggests several methods that have been developed to measure different types of drought. Drought indicators can be divided into two main categories, ground-based or satellite-based, depending on their derivation.

2.1 Ground-based Drought Indicators

Traditionally, meteorological drought indicators are based on direct ground measurement of climatic variables such as rainfall, evapotranspiration, and temperature (Steinemann et al., 2005). Most of them are driven by rainfall variations. Some of the widely used indicators include the Palmer Drought Severity Index (PDSI) (Palmer, 1965), the Standard Precipitation Index (SPI) (McKee et al., 1993), the Percent of Normal, and the Deciles approach (Gibbs and Maher, 1967). The PDSI is considered useful in monitoring drought at a regional scale and allows comparisons over relatively large zones (Steinemann et al., 2005). Compared to the PDSI, the SPI has a better statistical foundation (Robeson, 2008) and the capacity to reproduce both short-term and long-term drought impacts (Guttman, 1998; Hayes et al., 1999). The Percent of Normal indicator is a simple measure based on rainfall that can be applied for the analysis of single regions or seasons (Steinemann et al., 2005). The so-called Deciles technique was developed to overcome some of the drawbacks within the Percent of Normal approach. Both the SPI indicator and the Deciles technique have a better performance compared to the PDSI, according to six evaluation criteria (Keyantash and Dracup, 2002).

Hydrological drought sets slower and lasts longer compared to meteorological drought (Nagarajan, 2009). Some of the most widely used indices for hydrological drought are the Palmer Hydrological Drought Severity Index (PHDI) (Karl, 1986) and the Surface Water Supply Index (SWSI) (Shafer and Dezman, 1982). The former was developed to spot longer-term hydrological

effects, while the latter was designed to overcome some of the problems involved with the Palmer index (Steinemann et al., 2005).

Agricultural drought can be identified through the Crop Moisture Index (CMI) (Palmer, 1968). The index was developed to assess short-term moisture supply over major crop-producing areas.

2.2 Satellite-based Drought Indicators

Several indicators for drought monitoring can be derived from satellite-based information. The Rainfall Estimate (RFE) (Xie and Arkin, 1997) was developed to estimate precipitation over Africa and complement the information available from the sparse network of ground stations. The RFE combines information on cloud temperature and cold cloud persistence with rainfall measured by rain gauge stations. The Water Requirement Satisfaction Index (WRSI) (Frere and Popov, 1986) assesses a crop's performance during the growing season based on its water supply and demand. Adapted by the U.S. Geological Survey (USGS), the WRSI supports the monitoring requirements of the Famine Early Warning System Network (FEWS-NET) (Wardlow, 2009).

Persendt (2009) states that satellite-based drought indices can be divided into three groups: (i) indices based on the state of the vegetation, which are extrapolated using the reflective channels; (ii) indices based on surface brightness temperature, which is extrapolated from the thermal channels; and (iii) indices based on a combination of (i) and (ii). The first group includes indices such as the NDVI (Tucker, 1979), the Vegetation Condition Index (VCI) (Kogan, 1995), the Enhanced Vegetation Index (EVI) (Huete et al., 2002), and the Vegetation Productivity Indicator (VPI) (Al-Bakri and Taylor, 2003). The second group includes indices such as the Temperature Condition Index (TCI) (Kogan, 1997), and the third group includes indices such as the ratio between Land Surface Temperature (LST) and NDVI (Boegh et al., 1998), and the Vegetation Health Index (VHI) (Karnieli et al., 2006).

The NDVI has been proven to be closely related to vegetation-moisture conditions, even though the relatedness depends to some extent on the season taken into consideration (Ji and Peters, 2003).

It is well known that it is more likely to find a drought increase in an area where negative NDVI anomalies are recorded. Significant correlations have been found between NDVI and Green Cover, Leaf Area Index (LAI) and Yield (Nidumolu et al., 2008). NDVI responds to precipitation with different time lags (Justice et al., 1991) depending on environmental factors such as the soil type (Richard and Pocard, 1998).

2.3 Proposed Methodology for Drought Hazard Analysis

Hazard analysis can be improved by estimating the probability of a severe natural hazard to occur in the future. The analysis of extreme events would help to upgrade existing tools for drought early warning systems by identifying areas prone to a higher potential risk. In this sense, the extreme value theory comprises the necessary tools to model extreme events, which can provide information both on the return levels and return periods of a drought with a certain severity. The analysis of extremes for gridded data, i.e. over an entire region, has been applied in other studies to assess severe wind hazards (Sanabria and Cechet, 2010) or to investigate trends in Mediterranean temperatures (Efthymiadis et al., 2011). Our analysis is concerned with exploring and modeling negative extreme values of the ADVI, since the onset of drought conditions is more likely to occur when negative NDVI shifts are recorded (Shaheen and Baig, 2011).

We first run an Exploratory Data Analysis (EDA) in order to gain better knowledge of the temporal variability of the ADVI within pixels. The focus is given to the temporal variability of the available data as extreme value models are highly influenced by such variation. Then, we test two main approaches within the extreme value theory: the peak-over-threshold approach and the block-maxima approach. The performance of the two approaches is compared by checking the precision of return level estimates. In order to estimate return levels pixel per pixel, we implement an algorithm using a set of R functions (R Development Core Team, 2011). This marks a new approach for the assessment of drought risk in third-world countries and aims to integrate and

improve existing methodologies. It is particularly useful when applied to areas where crop represents a primary source of livelihood for its inhabitants.

3. Study Area and Data

3.1 Study Area

One of Africa's most drought ridden areas is the Horn of Africa, where Ethiopia represents the most populated nation. Over the last few decades, this entire area has been experiencing severe drought consequences (Chumo, 2011; Food and Agriculture Organization, 2011). Food insecurity in Ethiopia is caused by environmental and managerial factors including land degradation, periodical drought, poor and insufficient risk management, population pressure, and agricultural practices mostly based on rain-fed farming (The World Bank, 2011).

Fig. 1 shows the study area, which is the South Tigray zone within the Tigray region of Ethiopia.

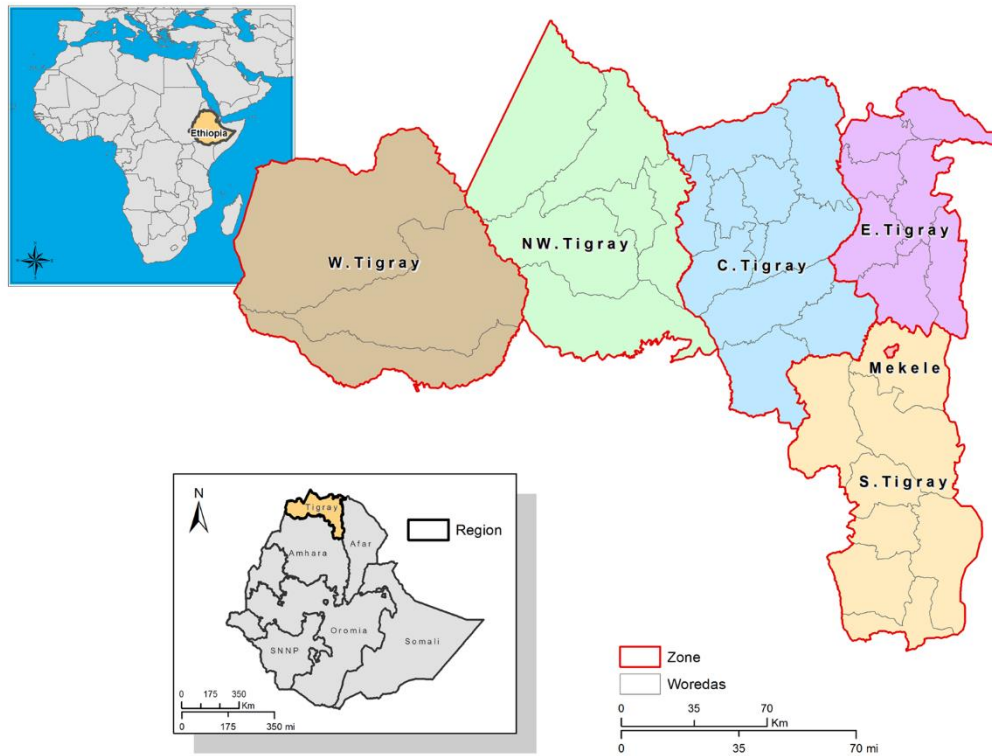


Figure 1 Tigray region, Ethiopia, and its administrative boundaries. Boundaries are represented according to the Global Administrative Unit Layers (GAUL) spatial database. Available in color online.

The Tigray region is composed of six zones and further subdivided into 35 small administrative districts called *woredas* (or *weredas*). A large part of the Tigray region is classified as cropland, thus periodically cultivated and utilized by the population as a source of food. The two main crop seasons are the *belgh* (short) and *meher* (main) seasons. *Belgh* rains are light and irregular, starting around March and ending around mid-May. The *meher* crop season is the main season and typically receives rainfall from June to early September. A delay in the onset of *belgh* and *meher* rains has led to severe consequences such as moisture stress, shortage of pasture for livestock, and a shift in planting with subsequent reduction of the growing period in which soil moisture was available for crop growth (Sewonet, 2002).

3.2 Available Data

The satellite images used for this study were kindly provided by the VITO organization, located in Belgium. The VEGETATION programme (VEGETATION, 2011) uses ground infrastructure

and two observation instruments, VGT1 and VGT2, on board SPOT 4 and SPOT 5 satellites, respectively. Satellite images are processed, archived, catalogued, and finally made available to VEGETATION users under certain conditions. The program provides daily global coverage at a spatial resolution of 1.15 km at nadir. The sensor is ideal for studies concerning long-term regional and worldwide environmental changes with regard to basic characteristics of vegetation cover. Images from April 1998 to January 2003 were recorded using the VGT1 sensor and from February 2003 to present using the VGT2 sensor. Differences between the two data sets are eliminated before making final products available to the user.

In this work, we use the SPOT-VGT S10 product (ten-day synthesis) from the first dekad of April 1998 to the third dekad of March 2009. Ten-day composite images are produced following a two-step procedure: first, segments (data strips) acquired over a ten-day period are merged; second, all segments are compared pixel per pixel in order to select the ‘best’ ground reflectance values. The compositing procedure seeks to eliminate distortions caused by factors such as atmosphere, aerosol scattering, snow, and cloud cover which reduce NDVI values in the visible and near-infrared channels (Wang and Tenhunen, 2004).

The Global Monitoring for Food Security (GMFS) agency bases its work on several indicators obtained by transforming the NDVI (ratio of difference between near-infrared and red channels over their sum) into difference-based indicators under consideration of historical values. The indicator selected for this work is the ADVI, which is defined as:

$$ADV I_x (y, p) = X(y, p) - \mu_x(p), \quad y = 1, \dots, N_y; \quad p = 1, \dots, N_p,$$

where y is the actual year, p is the actual time interval within year y , N_y is the last year of the time series, and N_p is the last reference time interval within a year. In this work, the reference time interval is a dekad. $X(y, p)$ is the actual NDVI value for year y and dekad p , $\mu_x(p)$ is the long-term historical average for the NDVI within the same dekad p , and N_p is equal to 36 (1 year = 36 dekads). The ADVI value represents a shift of the actual value from the historical average of the same dekad, thus showing positive or negative anomalies. That is, a positive shift indicates an increase in the vigor of vegetation compared with the long-term average, whereas a negative shift

indicates the opposite. Prior to the analysis, digital numbers (DN) were converted to ADVI values using the following conversion from the S10 product metadata file:

$$\text{ADVI} = - 1.25 + 0.01 * \text{DN}$$

4. Extreme Value Approaches

The extreme value theory deals with the modeling of extreme observations. The two main approaches used in the literature are: the Peak-Over-Threshold (POT) approach and the block-maxima approach. The former uses the Generalized Pareto Distribution (GPD) to model all observations exceeding a certain threshold. The latter uses the Generalized Extreme Value (GEV) distribution to model values found in the tails of the distribution of observed values.

4.1 Block-Maxima Approach

In this approach, extremes are studied through maxima recorded over a given time interval. Models are built over a sequence of maxima $M_n = \max\{ X_1, \dots, X_n \}$ (where n is the fixed number of observations within a chosen block of time) by assuming they are extremes of independent and identically distributed sequences of random variables. The fundamental asymptotic result in this regard is the so-called “three-types” theorem (Fisher and Tippett, 1928). It states that rescaled sample maxima $(M_n - b_n) / a_n$ (where $\{b_n\}$ and $\{a_n > 0\}$ are sequences of constants) converge in distribution to a variable with a distribution belonging to one of the following families: Gumbel, Fréchet, or Weibull. All three families can be encompassed within a single parametric family called Generalized Extreme Value (GEV), defined as:

$$G(z) = \exp\left\{-\left[1 + \xi\left(\frac{z - \mu}{\sigma}\right)\right]^{-1/\xi}\right\}, \quad (1)$$

defined on $\{z : [1 + \xi(z - \mu / \sigma)] > 0\}$, where $-\infty < \mu < \infty$, $\sigma > 0$ and $-\infty < \xi < \infty$. Parameter μ identifies the location and σ identifies the scale. ξ is a shape parameter determining the rate of tail decay, with $\xi > 0$ giving the Fréchet distribution, $\xi < 0$ the Weibull distribution, and $\xi \rightarrow 0$ corresponding to the Gumbel distribution. All the aforementioned concepts apply equally to a sequence of minima, since $\max\{X_1, \dots, X_n\} = -\min\{-X_1, \dots, -X_n\}$. Estimates of extreme quantiles of the distribution are then obtained by inverting (1):

$$z_p = \begin{cases} \mu - \frac{\sigma}{\xi} [1 - \{-\log(1 - p)\}^{-\xi}], & \text{for } (\xi \neq 0), \\ \mu - \sigma \log\{-\log(1 - p)\}, & \text{for } (\xi = 0), \end{cases} \quad (2)$$

where $G(z_p) = 1 - p$. z_p is called the return level (or return value) associated with the return period $1/p$. On average, the level is expected to be exceeded once every $1/p$ time intervals (e.g. years, weeks, months), depending on the chosen time unit. More precisely, z_p is exceeded by the annual maximum/minimum in any particular year with probability p . Maximum likelihood estimations (MLE) of z_p are obtained by substituting ML estimates of GEV parameters $(\hat{\mu}, \hat{\sigma}, \hat{\xi})$ into (2). Since return levels are functions of GEV parameters, we can use the so-called delta method to estimate approximate confidence intervals for z_p . Furthermore, by the delta method,

$$\text{Var}(\hat{z}_p) \approx \nabla_{z_p}^T \mathbf{V} \nabla_{z_p},$$

where \mathbf{V} is the variance-covariance matrix of $(\hat{\mu}, \hat{\sigma}, \hat{\xi})$ and $\nabla_{z_p}^T = \left[\frac{\partial z_p}{\partial \mu}, \frac{\partial z_p}{\partial \sigma}, \frac{\partial z_p}{\partial \xi} \right]$

evaluated at $(\hat{\mu}, \hat{\sigma}, \hat{\xi})$ (Coles, 2001).

4.2 Peak-over-threshold Approach

The peak-over-threshold approach is based on the second theorem in extreme value theory (Balkema and Haan, 1974; Pickands, 1975) and models excesses of a given threshold u . It has been shown that threshold excesses have a corresponding approximate distribution within the Generalized Pareto family:

$$H(y) = 1 - \left(1 + \frac{\xi y}{\tilde{\sigma}}\right)^{-1/\xi}$$

defined on $\{y : y > 0 \text{ and } (1 + \xi y / \tilde{\sigma}) > 0\}$, where $\tilde{\sigma} = \sigma + \xi(u - \mu)$. As for GEV models, we can obtain parameter estimates via MLE and calculate return levels with corresponding confidence intervals (Coles, 2001).

5. Exploratory Data Analysis

The temporal variability of data within the study area and their correlation structure is analyzed through the Autocorrelation Function (ACF) and Partial Autocorrelation Function (PACF) (Box and Jenkins, 1976). Fig. 2 (a-b) shows ACF and PACF plots, respectively, computed for the Alamata woreda. Time lags always reflect the chosen time unit, in this case a dekad. To check for the overall variability across the study area, all values obtained within each pixel are grouped at each time lag using boxplots.

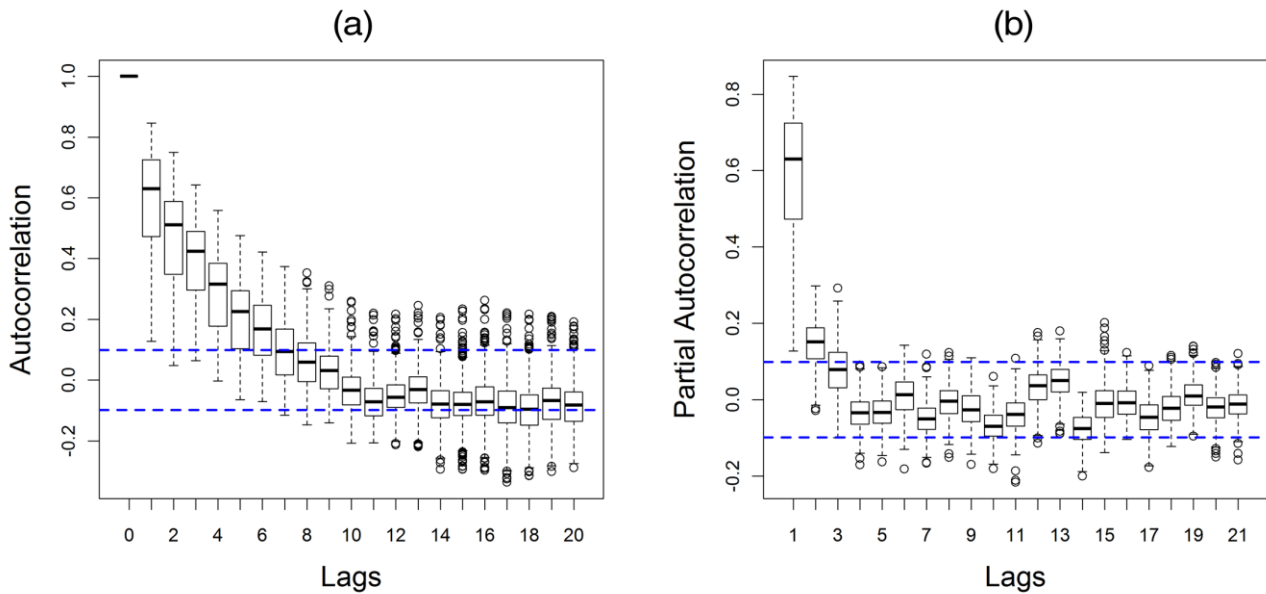


Figure 2 Temporal autocorrelation among observations within the Alamata woreda. (a) ACF-Boxplot. (b) PACF-Boxplot. Available in color online.

Both plots emphasize the presence of outliers at each lag. Boxplot medians shift inside the confidence interval bands starting from the seventh lag in the ACF and from the third lag in the PACF. These results suggest the presence of a significant correlation over time, thus raw observations have a marked temporal dependence. Replicating the same analysis on the remaining woredas revealed approximately the same temporal pattern. A strong dependence between observations would break one of the main assumptions upon which extreme value models are built. As a consequence, both parameter and return level estimates may be severely biased. At the same time, since the extreme value theory is based on asymptotic results, it is crucial to use a large sample size (as a general rule not below 30 units).

The block-maxima approach aims to build a statistical model exclusively for maxima/minima of a time series. In the case of this project, using annual minima would result in too short of a time series to give reliable results (11 years yield only 11 observations). Using belgh-meher season minima would also yield to the same number of observations. A useful compromise can be found by using monthly minima, which gives 132 observations (from 132 months). Fig. 3 (a-b) shows that, besides the presence of outliers, boxplot medians tend to shift within confidence interval bands

after the very first lags. This result suggests that monthly minima have a weak dependence over time.

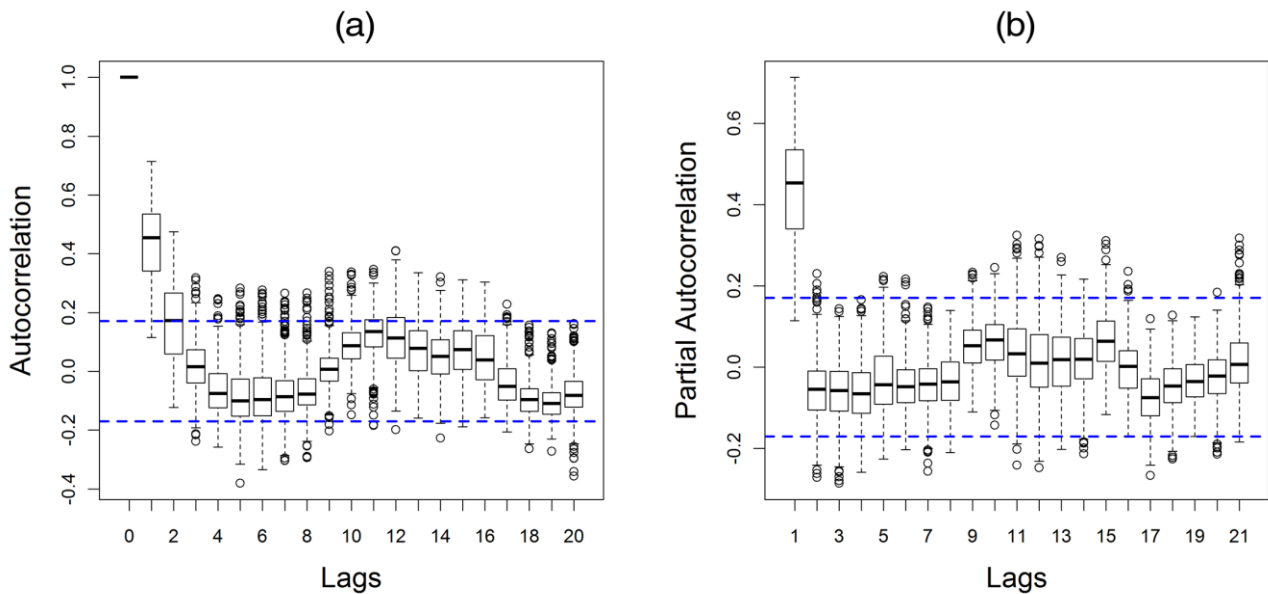


Figure 3 Temporal autocorrelation among monthly minima within the Alamata woreda. (a) ACF-Boxplot. (b) PACF-Boxplot. Available in color online.

Extreme value models typically require observations to be measured over contiguous and equal time intervals. Using unequal or not adjacent intervals is misleading and it becomes very difficult to correctly define and interpret return periods. Therefore, a partial time series made of monthly minima falling within the belgh-meher season is not recommended. However, we randomly sampled a few pixels within each woreda and verified that all parameter estimates of extreme value models are about the same when using all monthly minima versus only the ones within the cropping season.

6. Results and Discussion

The complete ADVI time series includes several zero or near-zero values. Most of them are outside the belgh-meher season because shifts from the historical average can be rarely observed outside the rain season. Indeed, irregular rainfall patterns represent the major source of variation for

ADVI values. The peak-over-threshold approach uses the Generalized Pareto Distribution (GPD) and takes into account all observations exceeding an appropriate threshold. Therefore, these models are potentially able to avoid the presence of zero values. However, as shown in section 5, consecutive dekadal observations are highly correlated over time and return level estimates may be severely distorted. Monthly minima, unlike dekadal observations, are weakly correlated over time, justifying our choice of using the block-maxima approach, expressed by Generalized Extreme Value (GEV) models. Other studies confirmed that peak-over-threshold models lack power when observations are strongly dependent (Malevergne et al., 2006) or when they are temporally clustered (Fawcett and Walshaw, 2007). The accuracy of return levels estimated with GPD and GEV distributions is assessed on a randomly selected pixel within the Alamata woreda, as shown in Fig. 4 and Fig. 5 respectively. We found similar behaviors in other randomly selected pixels within the same woreda and across all remaining woredas within the study area.

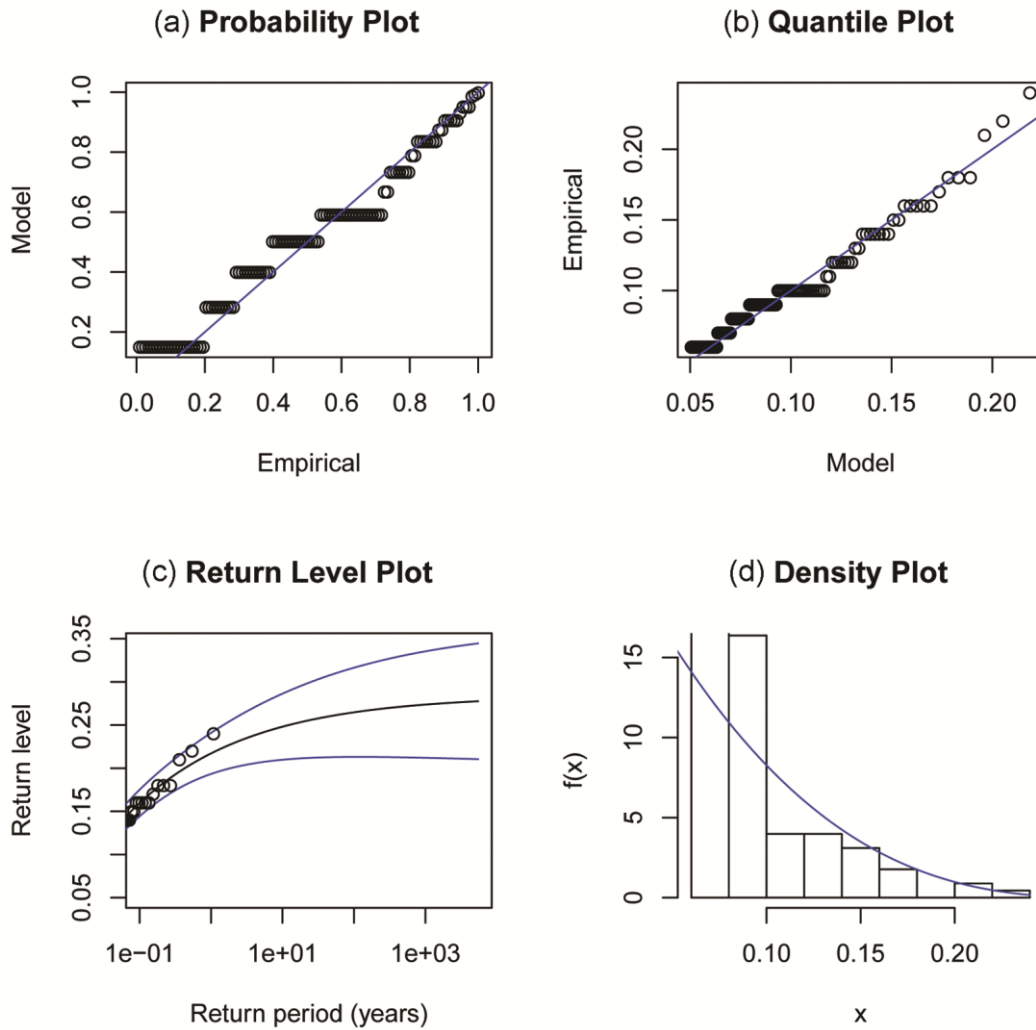


Figure 4 GPD model diagnostic with threshold -0.05 over pixel $n^\circ 22$, Alamata woreda. (a) **Probability plot:** cumulative frequencies are compared between empirical values (x -axis) and GPD theoretical values (y -axis). (b) **Quantile plot:** empirical quantiles (x -axis) are compared with quantiles of the GPD distribution (y -axis). (c) **Return Level Plot:** return periods (x -axis) and associated return level estimates (y -axis). In blue is the estimated confidence interval band. (d) **Density plot:** empirical histogram and GPD probability density function (in blue). Available in color online.

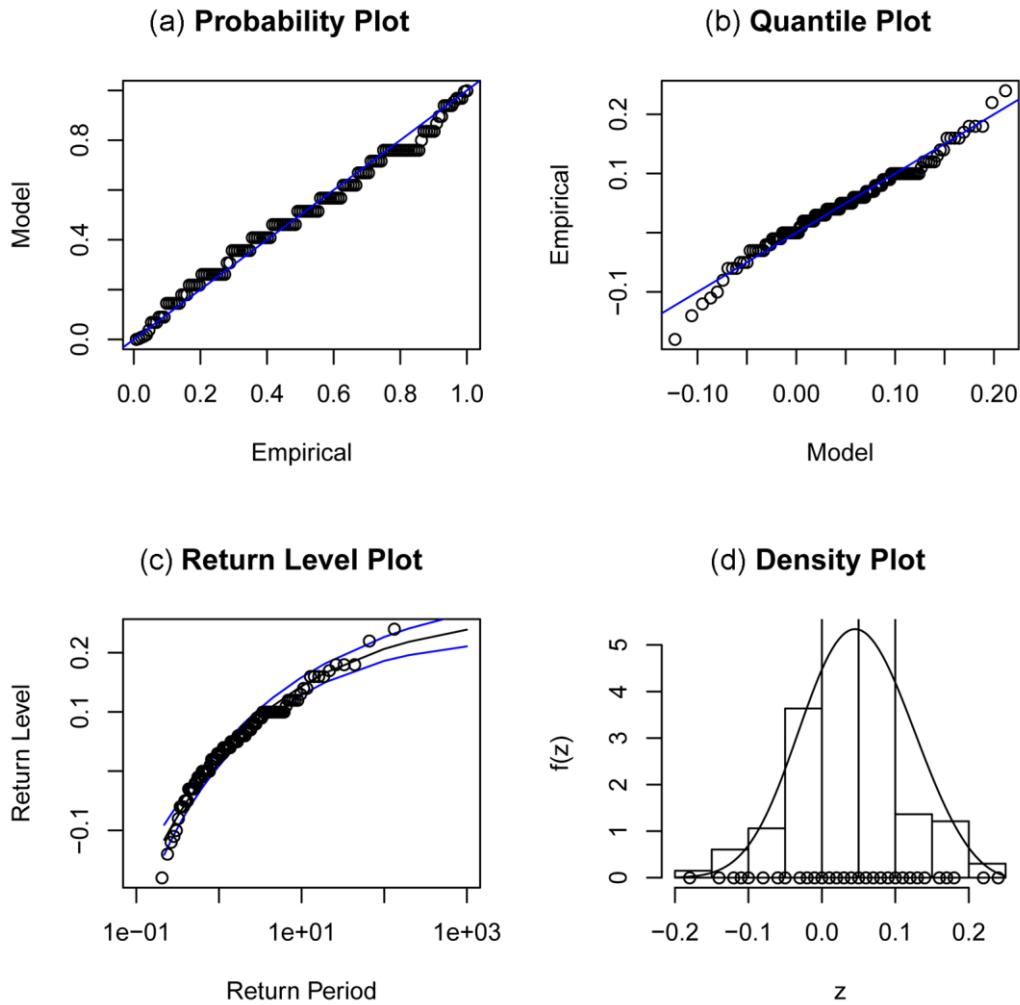


Figure 5 GEV model diagnostic over pixel n° 22, Alamata woreda. (a) Probability plot: cumulative frequencies are compared between empirical values (x -axis) and GEV theoretical values (y -axis). (b) Quantile plot: empirical quantiles (x -axis) are compared with quantiles of the GEV distribution (y -axis). (c) Return Level Plot: return periods (x -axis) and associated return level estimates (y -axis). In blue is the estimated confidence interval band. (d) Density plot: empirical histogram and GEV probability density function (in blue). Available in color online.

In Fig. 4, the return level plot appears to be correct because points lie entirely inside confidence interval bands. However, the upper left and right graphs show a bad model fitting to the time series of available data, meaning that parameter estimates for computing return levels are unreliable. Moreover, return level estimates stop around a five-dekad period (x -axis), representing a period too short (only one and a half months) to be considered of interest. All estimates after this time gap are completely unreliable and not useful for this work. Fig. 5 shows that GEV models have a better overall fitting to empirical values compared to GPD models. Return level estimates are sufficiently precise, except for a few points lying outside the confidence interval bands.

Fig. 6 (a-c) shows the estimated ADVI return levels at 10, 100, and 1000 months, respectively (i.e. approximately 1, 8, and 83 years). Fig. 7 (a-b) shows the estimated lower and upper confidence

intervals for the estimated ADVI 10-month return levels. Return level estimates are extremely precise, as demonstrated by the similarity between the original estimates and both lower and upper confidence intervals. Intervals based on profile likelihood are preferred for asymmetric data, which is not the case here since observations are mean-centered by construction. Moreover, the evaluation of different methods goes beyond the scope of this article. We observed a similar precision in the confidence intervals estimated for the 100-month and 1000-month return levels.

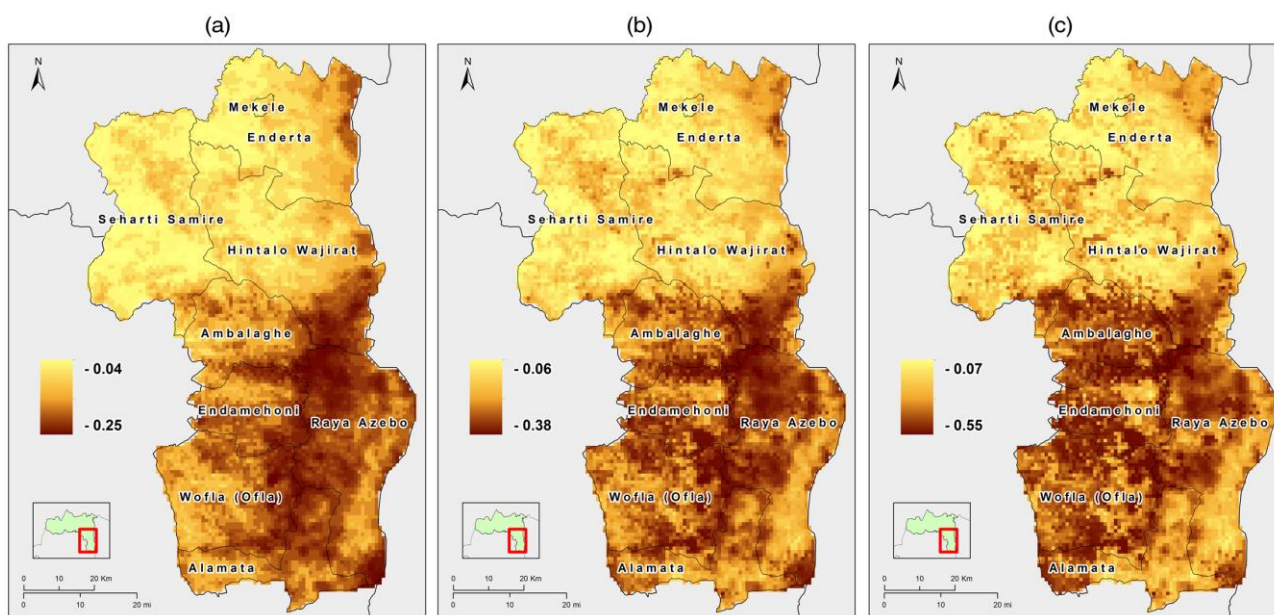


Figure 6 ADVI return level estimates. (a) 10-month return levels. (b) 100-month return levels. (c) 1000-month return levels. NOTE: the range of values shown in the legend differs for the three maps, hence bright and dark areas in one map do not necessarily have the same values in all the others. Available in color online.

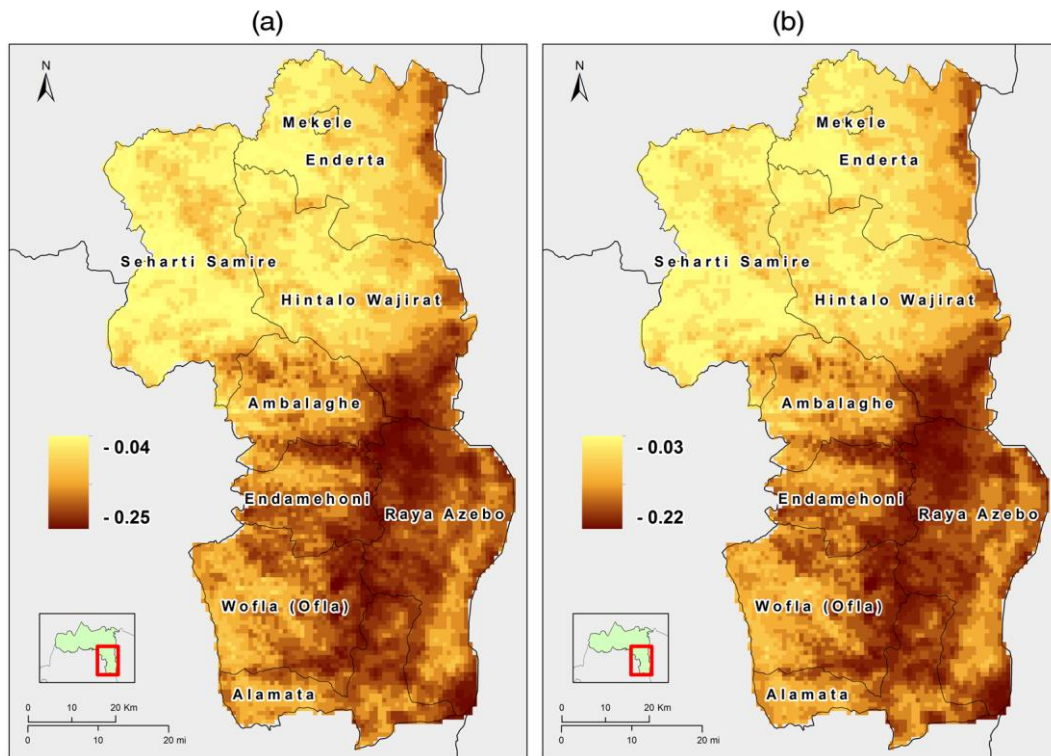


Figure 7 Confidence intervals for the estimated ADVI 10-month return levels. (a) Lower confidence intervals. (b) Upper confidence intervals. Available in color online.

Ten-month ADVI return levels are values associated with the return period 1/10 and are expected to be exceeded on average once every 10 months. In other words, those values have a 10% probability of being exceeded in any month. Darker areas correspond to larger negative values, signaling a higher drought risk. All three return level maps show a higher drought risk in the central and southern woredas of South Tigray. Specifically, the northern and western parts of the Raya Azebo seem particularly prone to negative NDVI anomalies, thus signaling a drought warning. There are many other areas that show either a short-range or a long-range tendency for drought risk, for example the Ambalaghe, Endamehoni, Wofla (Oflla) and Hintalo Wajirat (the southern part) woredas. The northern areas of South Tigray (with the exception of the north-eastern part of Enderta) seem less prone to be affected by short and long-term drought risk, in terms of a vegetation reduction.

Crop assessment reports are periodically published by the World Food Programme, the Joint Research Centre (JRC), and the Famine Early Warning System Network. Field observations, digital photos, and interviews with farmers are integrated with a few drought indicators such as the WRSI, the NDVI (absolute or as difference from the historical mean), and the VCI (derived from the

NDVI). All reports produced for Ethiopia in the past few years (2008-2010) confirm that South Tigray has been experiencing drought conditions: below normal rainfall conditions and, for several crop types, below normal vegetation conditions (MARS, 2008, 2009, 2010).

7. Conclusions

The purpose of this paper was to integrate and improve existing approaches for the quantification of drought risk in third-world countries by applying extreme value models on a pixel by pixel basis. Specifically, we proposed a new methodology to be implemented within hazard risk analyses. We overcome the scarcity of ground data by using satellite data, which have been proven to yield reliable indicators for drought monitoring. Although NDVI-related indicators do not differentiate between land cover types, they are generally good indicators of vegetation moisture conditions and respond to precipitation with varying time lags. Ten-day composite images partially avoid distortions affecting the quality of satellite data. Typical bias factors include the atmosphere, aerosol scattering, snow, and clouds. Our findings for the Ethiopian South Tigray zone are obtained by implementing an algorithm using a set of R software functions. The functions are easy-to-use, statistically sophisticated, and flexible enough to facilitate their use with other indicators in future applications and any set of return periods a researcher may be interested in. Finally, return levels could be inspected based on different soil types, agro-ecological zones, and cropping types. However, this goes beyond the scope of this work.

Acknowledgements

We would like to thank the VITO agency (Mol, Belgium) and in particular Sven Gilliams for providing us with SPOT-VGT satellite images and information regarding data collection procedures. We would also like to thank the United Nations World Food Programme and especially the VAM GIS group for collaborating with us on this project. Further, we want to thank Joanna

Syroka, Senior Program Advisor for the Climate and Disaster Risk Solution project (CDRS), for her helpful input throughout this work. The authors would like to thank both anonymous reviewers for their valuable comments and suggestions to improve the quality of the paper. The R code we developed for the main estimation routines is freely available at <https://github.com/ftonini/Extreme-Values-For-Gridded-Data>.

References

- Al-Bakri, J.T., Taylor, J.C., 2003. Application of NOAA AVHRR for monitoring vegetation conditions and biomass in Jordan. *J. Arid Environ.* 54 (3), 579-593.
- Balkema, A., Haan, L. de, 1974. Residual life time at great age. *Ann. Probab.* 2, 792-804.
- Boegh, E., Soegaard, H., Hanan, H., Kabat, P., Lesch, L., 1998. A remote sensing study of the NDVI-Ts relationship and the transpiration from sparse vegetation in the Sahel based on high resolution data. *Remote Sens. Environ.* 69, 224-240.
- Box, G.E.P., Jenkins, G.M., 1976. *Time series analysis: forecasting and control*. Holden-Day, Oakland, CA, U.S.A.
- Chumo, A.T., 2011. The horn of Africa drought: the endless plight. Webpage: <http://foreignpolicyblogs.com/2011/07/10/horn-africa-drought-endless-plight/>. Accessed March 21, 2012.
- Coles, S., 2001. *An introduction to statistical modeling of extreme values*. Springer Series in Statistics.
- Efthymiadis, D., Goodess, C.M., Jones, P.D., 2011. Trends in Mediterranean gridded temperature extremes and large-scale circulation influences. *Nat. Hazards Earth Syst. Sci.* 11, 2199-2214.
- Fawcett, L., Walshaw, D., 2007. Improved estimation for temporally clustered extremes. *Environmetrics* 18 (2), 173-188.
- Fisher, R.A., Tippett, L.H.C., 1928. Limiting forms of the frequency distribution of the largest or smallest member of a sample. *Math. Proc. Camb. Philos. Soc.* 24, 180-190.
- Food and Agriculture Organization, 2011. Drought-related food insecurity: a focus on the Horn of Africa. Emergency ministerial-level meeting. July 25, 2011.
- Frere, M., Popov, G., 1986. Early agrometeorological crop yield assessment. FAO Plant Production and Protection Paper No. 73, 144. Food and Agriculture Organization (FAO), Rome, Italy.
- Gibbs, W.J., Maher, J.V., 1967. Rainfall deciles as drought indicators. Bureau of Meteorology, Melbourne, Australia. Bulletin no. 48.
- Guttman, N.B., 1998. Comparing the Palmer drought Severity Index and the Standardized Precipitation Index. *J. Am. Water Resour. Assoc.* 34 (1), 113-121.
- Hayes, M.J., Svoboda, M., Wilhite, D.A., Vanyarkho, O.V., 1999. Monitoring the 1996 drought using the Standardized Precipitation Index. *Bull. Am. Meteorol. Soc.* 80 (3), 429-438.
- Huete, A., Didan, K., Miura, T., Rodriguez, E.P., Gao, X., Ferreira, L.G., 2002. Overview of the radiometric and biophysical performance of the MODIS vegetation indices. *Remote Sens. Environ.* 83, 195-213.
- Jensen, J.R., 2005. *Introductory digital image processing: a remote sensing perspective*, 3rd ed. Prentice Hall, Upper Saddle River, NJ, U.S.A.
- Ji, L., Peters, A.J., 2003. Assessing vegetation response to drought in the northern Great Plains using vegetation and drought indices. *Remote Sens. Environ.* 87 (1), 85-98.
- Justice, O., Digdale, G., Townshen, D.Y., Nallacott, A.S., Kumar, M., 1991. Synergism between NOAA/AVHRR and Meteosat data for studying vegetation development in semi-arid West Africa. *Int. J. Remote Sens.* 12 (13).
- Karl, T.R., 1986. The sensitivity of the Palmer Drought Severity Index and Palmer's Z-Index to their calibration coefficients including potential evapotranspiration. *J. Climate and Appl. Meteorol.* 25, 77-86.
- Karnieli, A., Bayasgalan, M., Bayarjargal, Y., Agam, N., Khudulmur, S., Tucker, C.J., 2006. Comments on the use of the Vegetation Health Index over Mongolia. *Int. J. Remote Sens.* 27 (10), 2017-2024.
- Keyantash, J., Dracup, A.J., 2002. The quantification of drought: an evaluation of drought indices. *Bull. Am. Meteorol. Soc.* 83 (8), 1167-1180.
- Kogan, F.N., 1995. Droughts of the late 1980s in the United States as derived from NOAA polar-orbiting satellite data. *Bull. Am. Meteorol. Soc.* 76 (5), 655-668.
- Kogan, F.N., 1997. Global drought watch from space. *Bull. Am. Meteorol. Soc.* 78, 621-636.
- Malevergne, Y., Pisarenko, V., Sornette, D., 2006. On the power of generalized extreme value (GEV) and generalized Pareto distribution (GPD) estimators for empirical distributions of stock returns. *Applied Financial Economics* 16 (3), 271-289.

- MARS, 2008. Crop monitoring in Ethiopia. MARS agrometeorological bulletin, Volume 2. Webpage: <http://reliefweb.int/node/275887/pdf>. Accessed March 26, 2012.
- MARS, 2009. Crop monitoring in Ethiopia. MARS agrometeorological bulletin, Volume 2. Webpage: <http://reliefweb.int/node/13648/pdf>. Accessed March 26, 2012.
- MARS, 2010. Crop monitoring in Ethiopia. MARS agrometeorological bulletin, Volume 1. Webpage: <http://reliefweb.int/node/367467/pdf>. Accessed March 26, 2012.
- McKee, T.B., Doesken, N.J., Kleist, J., 1993. The relationship of drought frequency and duration to time scales. 8th Conference on Applied Climatology. Anaheim, CA, U.S.A., January 17-22, pp. 179-184.
- Nagarajan, R., 2009. Drought assessment. Springer.
- NASA Earth Observatory, 2011. Drought: the creeping disaster. Webpage: <http://earthobservatory.nasa.gov/Features/DroughtFacts/>. Accessed October 10, 2011.
- Nidumolu, U., Sadras, V., Hayman, P., Crimp, S., 2008. Comparison of NDVI seasonal trajectories and modelled crop growth dynamics. Proceedings of the 14th Australian Agronomy Conference. Adelaide, South Australia, 21-25 September.
- NOAA National Climatic Data Center, 2011. Satellite-based drought indicators. Webpage: <http://www.ncdc.noaa.gov/climate-monitoring/dyk/satellite-drought>. Accessed October 10, 2011.
- Palmer, W.C, 1968. Keeping track of crop moisture conditions, nationwide: The new Crop Moisture Index. *Weatherwise* 21 (4), 156-161.
- Palmer, W.C., 1965. Meteorological drought. Research paper No. 45. U.S. Department of Commerce Weather Bureau, Washington, D.C., U.S.A.
- Persendt, F.C., 2009. Drought Risk Assessment using Remote Sensing and GIS to alleviate poverty. A case study of the Oshikoto region in Namibia. Conference on Applied Geoinformatics for Society and Environment (AGSE). Stuttgart University of Applied Sciences, Germany, August 20-21.
- Pickands, J., 1975. Statistical inference using extreme order statistics. *Ann. Stat.* 3, 119-131.
- R Development Core Team, 2011. A language and environment for statistical computing. R Foundation for Statistical Computing. Vienna, Austria.
- Richard, Y., Pocard, I., 1998. A statistical study of NDVI sensitivity to seasonal and interannual rainfall variations in Southern Africa. *Int. J. Remote Sens.* 19 (15), 2907-2920.
- Robeson, S.M., 2008. Applied climatology: drought. *Prog. Phys. Geography* 32 (3), 303-309.
- Sanabria, L.A., Cechet, R.P., 2010. Extreme value analysis for gridded data. International Congress on Environmental Modelling and Software Modelling for Environment's Sake, Fifth Biennial Meeting. Ottawa, Canada.
- Sewonet, A., 2002. Significant "meher" harvest reductions in the northeastern lowlands of Tigray and Amhara regions expected. Webpage: <http://reliefweb.int/node/107396>. Accessed October 10, 2011.
- Shafer, B.A., Dezman, L.E., 1982. Development of a Surface Water Supply Index (SWSI) to assess the severity of drought conditions in snowpack runoff areas. Proceedings of the Western Snow Conference. Fort Collins, CO, U.S.A., pp. 164-175.
- Shaheen, A., Baig, M.A., 2011. Drought severity assessment in arid area of Thal Doab using remote sensing and GIS. *Int. J. Water Resour. Arid Environ.* 1 (2), 92-101.
- Steinemann, A., 2003. Drought indicators and triggers: a stochastic approach to evaluation. *J. Am. Water Resour. Assoc.* 39 (5), 1217-1233.
- Steinemann, A.C., Hayes, M.J., Cavalcanti, L.F.N., 2005. Drought indicators and triggers, in: D.A. Wilhite (Ed.) *Drought and water crises: science, technology, and management issues*. CRC Press.
- The World Bank, 2011. Productive and Safety Net Project. Webpage: <http://go.worldbank.org/AH71AI0FS0>. Accessed October 10, 2011.
- Tucker, C.J., 1979. Red and photographic infrared linear combinations for monitoring vegetation. *Remote Sens. Environ.* 8, 127-150.
- United Nations World Food Programme, 2011. Food security analysis. Webpage: <http://www.wfp.org/food-security>. Accessed October 10, 2011.
- VEGETATION, 2011. Products - Vegetation System. Webpage: <http://www.spot-vegetation.com/>. Accessed October 10, 2011.
- Wang, Q., Tenhunen, J., 2004. Vegetation mapping with multitemporal NDVI in North Eastern China Transect (NECT). *Int. J. App. Earth Obs. Geoinf.* 6 (1), 17-31.
- Wardlow, D., 2009. Remote sensing and drought monitoring--an overview, options for Mali, and future directions. Drought Monitor Workshop. Bamako, Mali. September 14-17, 2009.
- Wilcox, R., 2009. Climate and disaster risk solutions. Project Briefing Note. The Rockefeller Foundation and the World Food Programme.
- Xie, P., Arkin, A., 1997. A 17-year monthly analysis based on gauge observations, satellite estimates, and numerical model outputs. *Bull. Am. Meteorol. Soc.* 78, 2539-2558.